NIST Special Publication 260-184

Method for Measuring the Volume of Nominally 100 µm Diameter Spherical Water-in-Oil Emulsion Droplets

John A. Dagata
Natalia Farkas
John A. Kramar

This publication is available free of charge from:
http://dx.doi.org/10.6028/NIST.SP.260-184

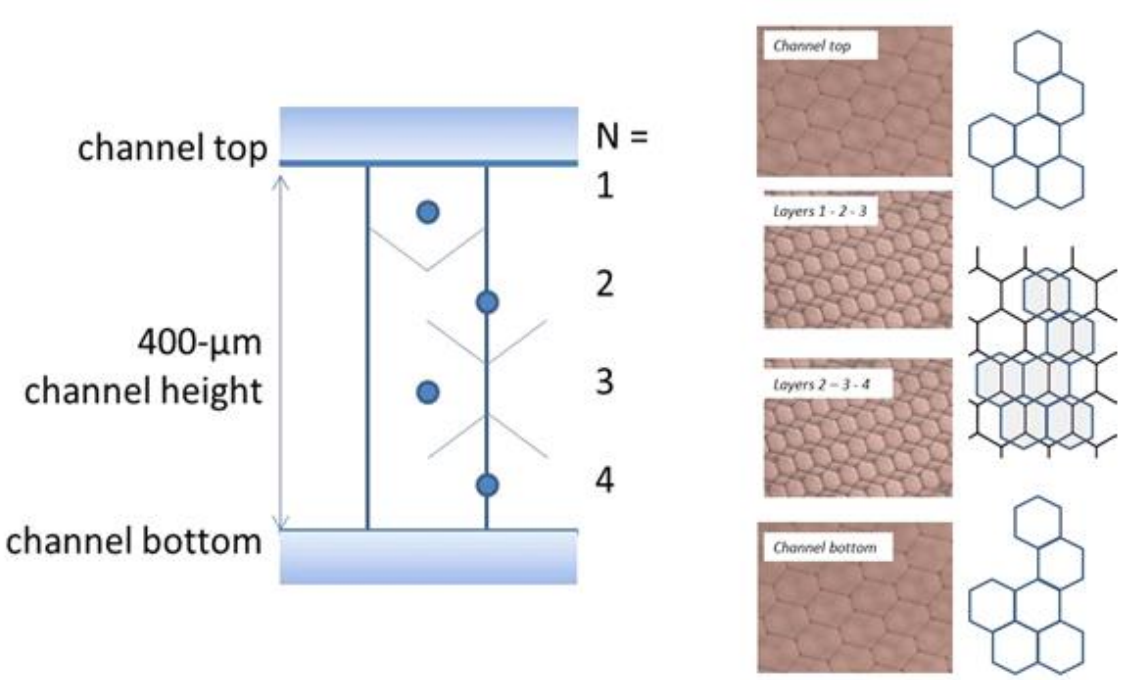

National Institute of Standards and Technology
U.S. Department of Commerce

NIST Special Publication 260-184

Method for Measuring the Volume of Nominally 100 µm Diameter Spherical Water-in-Oil Emulsion Droplets

John A. Dagata
Natalia Farkas
John A. Kramar
Engineering Physics Division
Physical Measurement Laboratory

This publication is available free of charge from:
http://dx.doi.org/10.6028/NIST.SP. 260-184

February 2016

U.S. Department of Commerce
Penny Pritzker, Secretary

National Institute of Standards and Technology
Willie May, Under Secretary of Commerce for Standards and Technology and Director

TABLE OF CONTENTS

Abstract ii
Keywords ii
Table of Contents ..... i L L
List of Tables Lv
List of Figures iv
Introduction 1
Measurand 1
Dilute method 1
Concentrated method 1
Calibration 3
Calibration of pixel size 3
Dimensional conformance of the Ibidi microfluidic channels by white-light interferometry 4
Channel-to-channel variation 5
Top and bottom surface variation 5
Traceable optical measurement of the microfluidic channel height 6
Membrane deformation 7
Measurement assurance 8
Measurement 9
Measurement of spherical droplets under dilute conditions 9
Measurement of the hexagonal unit cell under concentrated conditions 10
Determination of the volume fraction 12
Assumption of constant droplet volume 14
The unit cell as a quasi-equilibrium structure 14
Uncertainty analysis 16
Dilute method 16
Concentrated method 17
Type A: Sample emulsion preparation 17
Type A: Manufacturing 17
Type A: Measurement 17
Type B: Sample size distribution 17
Type B: Pixel calibration 17
Type B: Estimation of V_{HEX} 17
Type B: Manufacturing 18
Type B: Volume fraction 18
Combined Relative Standard Uncertainty 19
Validation 21
Comparison of Results from the Dilute and Concentrated Methods 21
Comparison with Literature Results 21
References 22

LIST OF TABLES

Table 1: NIST polystyrene latex (PSL) sphere SRMs for optical microscope calibration 3
Table 2: Pixel calibration results for optical microscope with three objectives 3
Table 3: WYKO Step height for Ibidi plates. 5
Table 4: 10X optical cross section results for channel height of channels 3 and 4 7
Table 5: 5X optical cross section results for step-height (total thickness) 7
Table 6: Samples 9
Table 7: Summary of mean spherical droplet volume as $V_{SPH} = \varphi D \cdot V_{HEX}$ measurements 15
Table 8: Uncertainty budget for dilute method of determining mean droplet diameter 16
Table 9: Uncertainty budget for concentrated method of determining mean droplet diameter 19
Table 10: Comparison of mean emulsion droplet diameter 21
Table 11: Evolution of mean droplet diameter and volume estimates 21

LIST OF FIGURES

Figure 1: Emergence of lattice domain structure across a microfluidic plate 2
Figure 2: Schematic of the Ibidi microfluidic channel plate 4
Figure 3: Cross sectional image of the microfluidic channel of nominally 400 μm channel height. ... 6
Figure 4: Optical image and droplet size distribution under dilute conditions. 10
Figure 5. Evolution of a close-packed droplet lattice in the microfluidic channel. 10
Figure 6. Interpretation of optical microscope images of the emulsion droplet tessellation. 11
Figure 7. Determination of the volume fraction using Princen's model 13
Figure 8. Measurement of the hexagonal unit cell out under quasi-equilibrium conditions. 13
Figure 9. Relationship between volume fraction and curvature parameter, r/a 14

INTRODUCTION

We report here two test methods for measuring the volume of emulsion droplets produced by the Bio-Rad QX100 digital droplet polymerase chain reaction (ddPCR) system with a DG8 emulsifying cartridge [1]. The dispersed aqueous phase of the water-in-oil emulsion consists of spherical droplets about 100 μm in diameter within which DNA substrates are condensed along with proprietary PCR reagents. Both methods are intended to provide a traceable and statistically meaningful volume determination of the droplets in order to certify the DNA concentration, i.e., the initial number of copies of a specific DNA target amplified in a PCR reaction. Adequate specification of the test material includes the nature of the DNA, the proprietary reagents used in the formulation, and the system used to generate the emulsion.

Measurand

The intended measurand, $\bar{V}_{SPH}$, is the mean equivalent spherical volume of aqueous emulsion droplets, $\bar{V}_{SPH} = 4/3 \cdot \pi \cdot R^3$, where $R = d/2$ is the radius and d the diameter of the droplet. Both methods use optical microscopy to obtain this mean volume of these nominally 100 μm diameter spherical droplets.

Dilute method

Assuming that the droplet shape is spherical, the radius *R*, or diameter *d*, can be estimated directly from optical measurements of dilute droplets within a microfluidic channel of an Ibidi #80621 μ-Slide VI-flat hydrophobic microfluidic plate [2]. Optical microscopy is generally considered an appropriate method for determining the mean volume of a spherical droplet existing in an emulsion. It seems a simple matter to measure the diameter of (nearly) perfectly spherical droplets in solution [3,4,5]. However in the case of this proprietary emulsion, there are concerns that 1) buoyancy of the droplets deforms the droplets so that their shape is no longer spherical; 2) there is a lack of optical contrast at the boundaries of the droplets due to multiple oil-water interfaces, making edge determination highly uncertain; 3) particle-particle contact makes definition of an area-equivalent spherical diameter difficult; and 4) individual-particle diameter measurements become time consuming for statistically meaningful sampling. Previous work suggests a deviation of 3 % to 4 % from sphericity which introduces a large error into uncertainty analysis [5].

Concentrated method

We propose an alternative approach to droplet volume measurements. Close-packed spherical emulsion droplets confined within a microfluidic channel transform into a space-filling polygonal lattice as the oil phase evaporates. The microfluidic channel height determines the resulting lattice dimensions such that the mean droplet volume is traceable to the unit of length. An optical micrograph of this lattice structure is presented in Figure 1.

The lattice is further defined as a hexagonal unit cell. Droplet volume is conserved during this shape transformation, which we write as $\bar{V}_{SPH} = \varphi_D \cdot \bar{V}_{HEX}$, where the volume of the hexagonal unit cell, reduced by the volume fraction of dispersed (aqueous) droplet phase, φ_D, yields an estimate for the mean spherical droplet volume in solution. The latter term accounts for the hexagonal unit cell encompassing the *total* volume of both aqueous and oil phases, i.e., $\varphi_D + \varphi_C = 1$, with φ_C the continuous (oil) phase.

Figure 1: Emergence of lattice domain structure across a microfluidic plate.
Channel dimensions ($L \times W \times H$) of the Ibidi #80621 μ-Slide VI-flat hydrophobic are nominally 17 mm × 3.8 mm × 400 μm. The mean diameter of the self-assembled aqueous emulsion droplets is on the order of 100 μm.

Calculation of $\bar{V}_{HEX} = N_L^{-1} \cdot h \cdot \bar{A}_{HEX}$ is straightforward and depends on the number of layers, N_L, in the lattice formed within a microfluidic channel of height, h, and the hexagonal cross- sectional area, $\bar{A}_{HEX}$. Under steady-state temperature and pressure conditions, the microfluidic channel height represents the space between fixed boundaries which uniquely determines the hexagonal unit-cell. Thus the mean droplet volume is ultimately traceable to the unit of length by determination of the microfluidic channel height.

We are interested in the limit in which $\varphi_D \rightarrow 1$, i.e., the condition corresponding to almost complete draining of the oil phase. The remaining oil phase is present in so-called Plateau borders, the collapsed border channels at the edges and interstices of tessellated droplets. Considerable effort has been made to characterize geometric and force balance requirements under these conditions for foams and emulsions [6,7,8].

CALIBRATION

The height of the microfluidic channel, *h*, is the essential link between the mean droplet volume and the standard unit of length. This link is established with NIST standard reference materials to calibrate the pixel size of an optical microscope/camera system. This system is used to determine the mean channel height and then, in an independent set of measurements, directly obtain the dimensions of the hexagonal unit cell. White-light interference microscopy was performed in order to validate the quality of the cross-sectional measurements and provide additional geometrical information about the channels.

Calibration of pixel size

A Mitutoyo long-working distance reflection optical microscope equipped with a (1600 × 1200) pixel Pixelink CCD camera was used to establish a mean traceable value of the channel height. Pixel calibration for 5X, 10X, and 50X microscope objectives used in this study was performed using NIST SRM polystyrene latex (PSL) spheres. Highly ordered 2Dimensional lattices of PSL spheres were prepared on mica substrates and line averages of 10 or more spheres were obtained from micrographs using ImageJ analysis software [9]. The PSL SRMs are described in Table 1. The pixel calibration results are summarized in Table 2.

Table 1: NIST polystyrene latex (PSL) sphere SRMs for optical microscope calibration

SRM	Nominal diameter	Certified diameter	Year issued
1690	1 μm	0.895 ±0.005 μm	1982
1692	3 μm	2.982 ±0.016 μm	1991

Table 2: Pixel calibration results for optical microscope with three objectives

	Results of Pixel Size Measurements		
Objective	Mean	SD	CV[a]
50X	0.0786 μm	0.000236 μm	0.03 %
10X	0.3943 μm	0.000394 μm	0.10 %
5X	0.7877 μm	0.000315 μm	0.04 %

a $\mathrm{CV} \equiv 100 \cdot \mathrm{SD}/\mathrm{Mean}$

Dimensional analysis was carried out based on pixel counts initially and converted into a reference unit of length using the above information before final data processing. Measurement uncertainty associated with the calibration spheres is reported in the NIST SRM Certificates of Analysis [10,11] and is about 0.5 % for both diameter spheres. An estimate of pixel calibration at 10X is obtained by recognizing that the mean diameter of one calibration sphere is 10 pixels and an uncertainty arises in the two outermost pixels of the imaged spheres on the scale of the calibration standard. Thus the uncertainty is (2/10)×(0.5 %) = 0.1 %. This estimate agrees with the measured relative standard deviation of a mean pixel with the 10X objective.

Dimensional conformance of the Ibidi microfluidic channels by white-light interferometry

Use of a global mean value for the height of the microfluidic channel is based on the assumption that local variation in the nominal 400 µm height is insignificant: 1) along the 17 mm length and across the 3.8 mm width of a given channel; 2) among the channels of a given plate; and, 3) for all plates from the same lot number. Figure 2 provides a schematic of the Ibidi microfluidic plate.

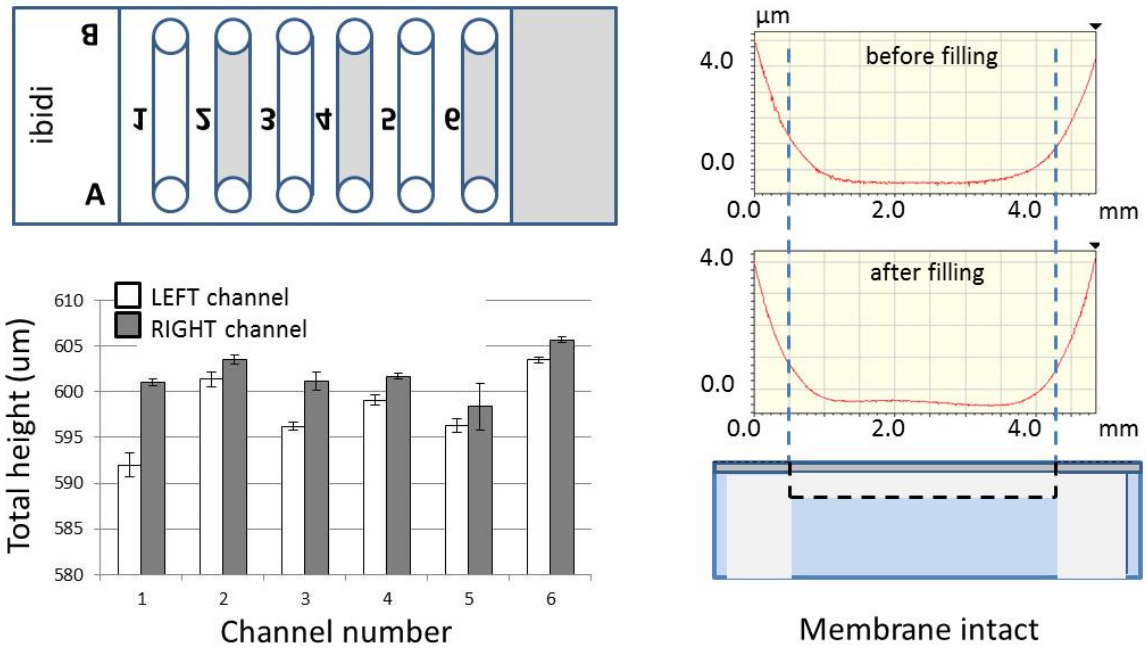

Figure 2: Schematic of the Ibidi microfluidic channel plate.

WYKO interference microscope measurements were made along the left and right channel edges for all six channels. Mean total height of the nominally 400 µm channel plus 200 µm thick membrane step height is reported. The step height was created by carefully removing the membrane from the channel. Possible deformation of the membrane due to filling and evaporation of the emulsion oil phase was also investigated.

The WYKO surface profiler [12] is a non-contact optical profiler used to measure surface roughness and step height. Vertical scanning interferometry mode was used for the measurements reported here. In this technique, unfiltered (white) light is separated by a beam splitter into two paths. Reflected light from a reference mirror recombines with light reflected from the sample surface as a calibrated piezoelectric transducer scans the focal point of the microscope, producing a set of interference fringes at best focus. Fringe analysis of images collected along a sequence of focal points provides the mean height difference of features on the sample surface and average roughness of the entire sample or specific sub-regions.

The WYKO microscope was calibrated using an in-house (10.55 ±0.05) µm step-height standard. The microscope was used with a 2.5X objective with 0.5 reduction lens, providing a field of view of (4.8 × 3.7) mm^2 along the X and Y axes, respectively. The CCD camera contained (736 × 480) pixels. Step heights were collected and the data plane fit and averaged over all pixels.

Channel-to-channel variation

The WYKO instrument was used to sample plate-to-plate and channel-to-channel variation of the step height, i.e., the sum of the channel height and the membrane thickness, at locations along the left and right sides of the channel by gently removing the membrane with tweezers. Images were taken along both sides of three channels from two Ibidi #80621 (lot number 140203/2) plates each. Six locations per channel were measured for a total of $N = 36$ locations. The mean step height results are summarized in Table 3.

Table 3: WYKO Step height for Ibidi plates.
The field of view at each location is 4.8 mm × 3.7 mm

		Left-hand side of channel			Right-hand side of channel		
Plate	Channel	Locations	Mean	SD	Locations	Mean	SD
4	1	3	592.0 μm	1.3 μm	3	601.0 μm	0.4 μm
	3	3	596.2 μm	0.5 μm	3	601.2 μm	1.0 μm
	5	3	596.3 μm	0.7 μm	3	598.4 μm	2.6 μm
5	2	3	601.4 μm	0.8 μm	3	603.5 μm	0.5 μm
	4	3	599.1 μm	0.6 μm	3	601.7 μm	0.3 μm
	6	3	603.5 μm	0.3 μm	3	605.7 μm	0.3 μm
Subtotals		18	598.1 μm	3.8 μm	18	601.9 μm	2.3 μm
Combined		36	600.0 μm	3.1 μm			

The variation from left to right across the width of the channel is only 0.25 % of the channel height. However, this small difference between the left- and right-hand side step heights, 598 μm vs. 602 μm, obscures a systematic channel-to-channel variation across the plate as seen in the histogram presented in Figure 2. A rather large left-right discrepancy was obtained routinely for channel #1 and an above-average step height was obtained for channel #6. Since channels #3 and #4 exhibited the best left-right uniformity, these channels were used for all droplet volume determination based on the hexagonal unit cell. However, no statistically significant differences in estimated droplet volume were observed when channels #2 and/or #5 were used.

Top and bottom surface variation

A key assumption of the proposed method requires that the top and bottom surfaces of the microfluidic channel are fixed boundaries. These boundaries allow the parameters N_L, h, and $\bar{A}_{HEX}$ of the hexagonal unit cell to be defined. In addition to requiring that the left- and right-hand side of the channels are sufficiently constant to make the use of a mean channel height possible, variations of the local channel height due to surface roughness and flatness of the top and bottom surfaces must be investigated. Measurement of the top membrane surface of two channels using the WYKO instrument indicated a surface roughness, $R_q = 0.27$ μm. The flatness across a central 3 mm portion of the 3.8 mm wide channel, was < 0.2 μm or essentially unmeasurable.

In order to make WYKO measurements of the bottom channel surface, the membrane was removed with tweezers. This surface has occasional tool marks running parallel to the long channel axis, though not as obvious as the tool marks observed along the channel side walls shown in Figure 3. For the bottom channel surface, $R_q = 0.60$ μm and the flatness was again too small to estimate. These results are for low spatial frequencies only.

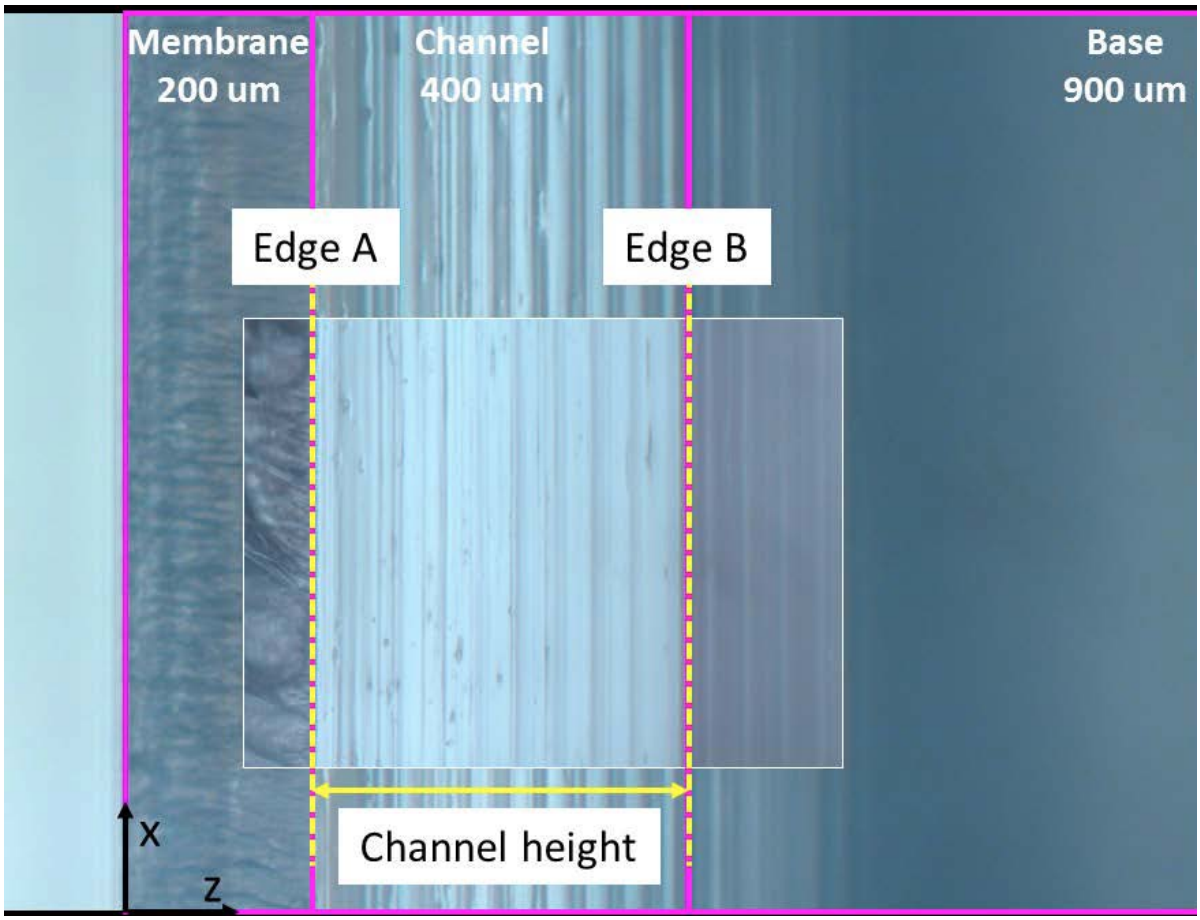

Figure 3: Cross sectional image of the microfluidic channel of nominally 400 µm channel height. From top to bottom, dashed yellow lines identify the nominally 200 µm thick membrane with vertical crazing, the side of the channel with a identifiable by horizontal tool marks, and finally the base plate which is out of focus in this image.

Traceable optical measurement of the microfluidic channel height

The height of the microfluidic channel is the essential link between the mean droplet volume and the standard unit of length. Determination of a mean channel height is based on sampling plates from the same lot number. For this measurement, the 200 µm thick membrane making up the upper surface of the channel was carefully removed with tweezers and each plate was cross sectioned along the long axis of every channel to be tested. Both sides of the channel were then imaged edge-on. One such image is shown in Figure 3**,** where the nominally 400 µm channel height can be associated with grooved tool marks running horizontally along the side of the channel. The intersection of the channel side with the nominally 200 µm thick membrane, at the upper interface, and with the base of the plate (identified by an optical sidewall reflection), at the lower surface, are indicated by yellow dashed lines in the figure. Crazing of the membrane, perpendicular to the tool marks makes it particularly easy to identify the upper interface.

Three Ibidi #80621 (lot number 140203/2) plates were selected and two to four channels per plate were evaluated. Images were taken at ten locations along the left- and right-hand sides of each channel. Detailed measurement results for the channel height obtained at 10 times (10X)

magnification are presented in Table 4. Detailed measurement results for the total thickness obtained at 5X magnification are presented in Table 5.

Table 4: 10X optical cross section results for channel height of channels 3 and 4
Results in *italics* are not included in statistical summaries.

		Left-hand side of channel			Right-hand side of channel		
Plate	Channel	Locations	Mean	SD	Locations	Mean	SD
1	*1*	*5*	*389.4 μm*	*3.8 μm*	*5*	*390.6 μm*	*3.1 μm*
	2	*5*	*391.7 μm*	*1.2 μm*	*5*	*393.5 μm*	*2.3 μm*
	3	5	392.6 μm	1.0 μm	5	393.1 μm	2.3 μm
	4	5	394.7 μm	2.3 μm	5	393.1 μm	1.4 μm
2	*2*	*5*	*389.0 μm*	*6.7 μm*			
	3	5	390.6 μm	2.5 μm			
	4	5	390.6 μm	3.5 μm			
3	3	5	396.1 μm	0.8 μm	5	395.1 μm	0.7 μm
	4	5	395.9 μm	1.2 μm	5	391.2 μm	2.5 μm
Subtotals		30	393.4 μm	2.3 μm	20	393.1 μm	1.4 μm
Combined		50	393.3 μm	1.9 μm			

Table 5: 5X optical cross section results for step-height (total thickness)

		Left-hand side of channel			Right-hand side of channel		
Plate	Channel	Locations	Mean	SD	Locations	Mean	SD
1	1	2	598.2 μm	3.9 μm	5	600.3 μm	1.0 μm
	2	5	599.4 μm	1.7 μm	2	600.6 μm	1.7 μm
	3	5	598.3 μm	0.4 μm	4	600.0 μm	2.1 μm
	4	4	597.6 μm	0.8 μm			
2	2	5	602.2 μm	3.8 μm	2	603.7 μm	1.7 μm
	3	4	597.0 μm	0.6 μm	5	601.8 μm	4.5 μm
	4	2	599.8 μm	0.6 μm	4	597.2 μm	1.7 μm
3	3	3	600.2 μm	0.8 μm	1	599.4 μm	
	4	2	601.0 μm	1.1 μm	5	600.0 μm	0.7 μm
Subtotals		32	599.3 μm	1.6 μm	28	600.4 μm	1.7 μm
Combined		60	599.8 μm	1.7 μm			

There are no statistically significant differences in channel height or total thickness between the left- and right-hand sides of the channels. This step-height result agrees well with the WYKO step-height measurement, giving confidence to the mean channel height determination.

Membrane deformation

The mean membrane thickness of the microfluidic channel can be estimated from cross-sectional optical and WYKO results given in the above Tables: 206.5 ±2.0 μm. Because the membrane is relatively thin and composed of a relatively soft plastic material, it is prudent to determine the deformation induced during filling and drying of concentrated emulsion. The intact membrane covering two separate channels, one a #3 channel and the other a #4 channel, was imaged using the WYKO instrument. The surface roughness, R_q, and flatness across the central 3 mm portion of the

3.8-mm wide membrane were determined. Channels were then filled with emulsion solution and allowed to sit at ambient temperature and pressure for two hours before the parameters were again measured. A slight distortion of the membrane developed. For the two cases, membrane flatness before filling was not measurable above the surface roughness. After filling, one side of the membrane was raised relative to other by $\delta \approx 0.25$ μm in one case and $\delta \approx 0.5$ μm in the other. This is illustrated in Figure 2. Data along either edge of the cross section is artificially distorted by the plane fitting algorithm.

Measurement assurance

The instruments used in this study are located in laboratories that are temperature and humidity controlled with long-term conditions maintained at 23 ±1 ^{o}C and 28 ±8 % relative humidity. These conditions are monitored on a daily basis and measurements are not performed if conditions are outside these limits. This usually only occurs during annual site-wide maintenance events. Once the room environment has returned to these normal operating conditions, a period of 3 days is given before measurements are resumed.

For the measuring instruments covered in this document, validation of instrument performance within specified operational guidelines is carried out by performing a series of test measurements using a series of well-established certified reference materials produced, procured, and maintained by NIST staff.

The mean pixel size of the Mitutoyo optical microscope was checked just prior to recording of measurements using an in-house magnification standard which had previously been calibrated against the NIST PSL SRMs 1690 and 1692. Often the calibration was checked again at the end of the measurements. A control chart of these measurements is maintained in the laboratory housing the microscope.

Traceability is established through the use of calibration artifacts. Each instrument is therefore considered to be covered by “calibrate on use” requirements, i.e., each daily period a measurement process is executed.

MEASUREMENT

Emulsions were freshly prepared using a Bio-Rad QX100 droplet digital polymerase chain reaction (ddPCR) system and DG8 cartridge according to the manufacturer's specifications using its proprietary materials and measured on the same day. [1] Ibidi #80621 μ-Slide VI-flat hydrophobic microfluidic plates [2] from the same lot number were used for all droplet measurements.

Samples are given a unique sequence to identify the source, the origin of the DNA, the proprietary reagent used to generate the emulsion (see below), and a preparation date (e.g., 02/04/2015). Two types of DNA sample, human genomic [13] and a bacterial artificial chromosome containing cytomegalovirus (CMV) DNA [14], were formulated using one of two proprietary "mastermix" reagents: "Bio-Rad ddPCR Supermix for Probes" [15] and "ddPCR Supermix for Probes (no dUTP)" [16]. We refer to these mastermixes containing, or not containing, deoxyuridine triphosphate, as "with dUTP" and "no dUTP".

These mastermixes may have different chemical composition and physical properties that may affect the mean droplet size produced within the emulsifying cartridge. The continuous (oil) phase consisted of proprietary QX100 droplet generator oil available from the manufacturer. Table 6 lists the materials used to characterize the droplet volume measurement methods described in this report.

Table 6: Samples

TEST ID	Sample ID	Date	DNA	Mastermix
2013	645-1-12/19/2014	12/19/2014	Human genomic	with dUTP
2013	645-1-03/17/2015	03/17/2015	Human genomic	with dUTP
2013	645-1-03/20/2015	03/20/2015	Human genomic	with dUTP
2013	645-2-02/04/2015	02/04/2015	Human genomic	no dUTP
2013	645-2-02/10/2015	02/10/2015	Human genomic	no dUTP
2013	645-2-02/12/2015	02/12/2015	Human genomic	no dUTP
2014	645-3-02/24/2015	02/24/2015	CMV	with dUTP
2014	645-3-02/27/2015	02/27/2015	CMV	with dUTP
2014	645-3-03/03/2015	03/03/2015	CMV	with dUTP
2014	645-4-03/11/2015	03/11/2015	CMV	no dUTP
2014	645-4-03/12/2015	03/12/2015	CMV	no dUTP

Measurement of spherical droplets under dilute conditions

Previous estimates of the mean droplet volume were obtained from optical measurements of droplet diameter of highly dilute, 2D droplet arrays [3,4,5]. For this measurement, the emulsion must be diluted carefully with the oil phase to avoid coalescence of the droplets. We follow the procedure given in the literature by carrying out dilution within the microfluidic channel. First, 40-μL of oil-only solvent is introduced into a channel port followed by gentle injection of a small volume of the emulsion mixture. Rafting into 2D close-packed arrays occurs spontaneously or with slight agitation of the plate. Optical images were taken with the 10X microscope objective. An example of a highly dilute droplet array is shown in Figure 4a. As the volume of injected emulsion is increased, denser packing occurs and eventually multiple layers of a 3D lattice can be observed. Analysis of these optical images relies on a cross-sectional measurement for isolated droplets or at higher

concentration, a line average approach consisting of ten or more droplets for 2D and 3D arrays may be used.

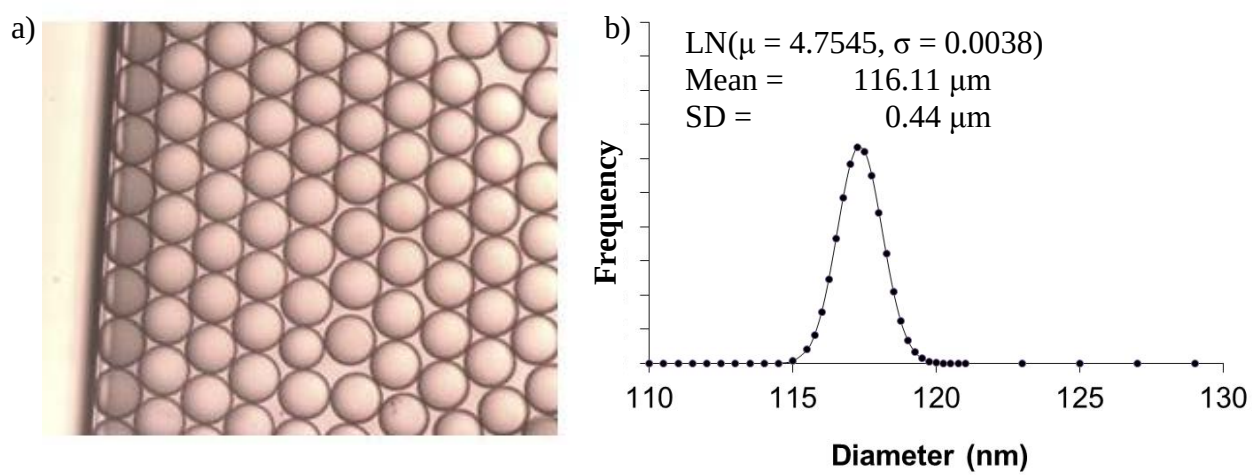

Figure 4: Optical image and droplet size distribution under dilute conditions.

a) Optical image of emulsion droplets in a microfluidic channel obtained under highly dilute conditions.
b) Particle size distribution of droplet diameter (sample 645-1-12/19/2015) determined by lognormal fitting parameters. Mean and SD are linear-space transformations of the lognormal μ and σ parameters.

Measurement of the hexagonal unit cell under concentrated conditions

40-μL of a freshly prepared emulsion solution is injected into a microfluidic channel of an Ibidi #80621 μ-Slide VI-flat hydrophobic microfluidic plate [2], leaving the filling ports open to the atmosphere. Over a period of a few hours the oil phase drains from the channel and evaporates and menisci appear at both open ends of the channel. Surface tension condenses the aqueous droplet-rich phase at or near the mid-point of the channel leading to increased crowding of aqueous droplets. The transformation of close-packed spherical droplets first into a rhombic dodecahedron unit cell and then into a truncated octahedron (or Kelvin cell) is a function of the volume fraction of the dispersed phase, φ_D. This process is illustrated in a top-down view in Figure 5. Figure 1 illustrates domain formation across the entire microfluidic channel.

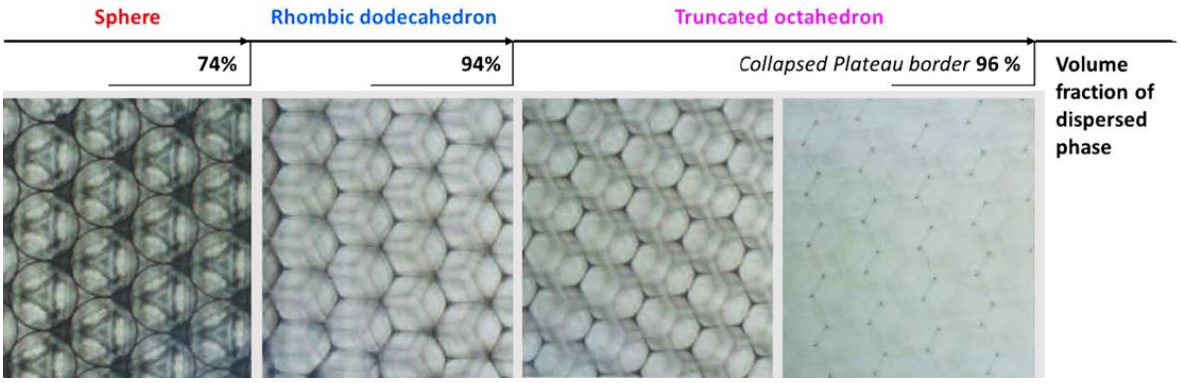

Figure 5. Evolution of a close-packed droplet lattice in the microfluidic channel.

Droplet shape undergoes a spherical-to-polygonal transformation at constant volume as the volume fraction of the dispersed (aqueous) phase increases as a result of draining of the continuous (oil) phase. The time required to attain collapsed Plateau border channels (volume fraction $\varphi > 96$ %) at ambient temperature and pressure is approximately 2 hours. This transformation is fully reversible by addition of solvent, i.e., the oil phase.

The microfluidic channel height, nominally h = 400 μm, can accommodate a 3D lattice of ≈100 μm diameter aqueous droplets where the layer number N_L is expected to be 4. That four droplets indeed occupy alternating lattice positions is verified by changing the focal point of the microscope stepwise through the channel (microscope Z axis). A schematic of the tessellating structure is presented in side view in Figure 6a. Optical images at the top and bottom of the channel show flattened droplets forming a simple hexagonal tiling and three intermediate tessellating regions between the four droplet layers which reveal an unambiguous Kelvin-cell projection, Figure 6b.

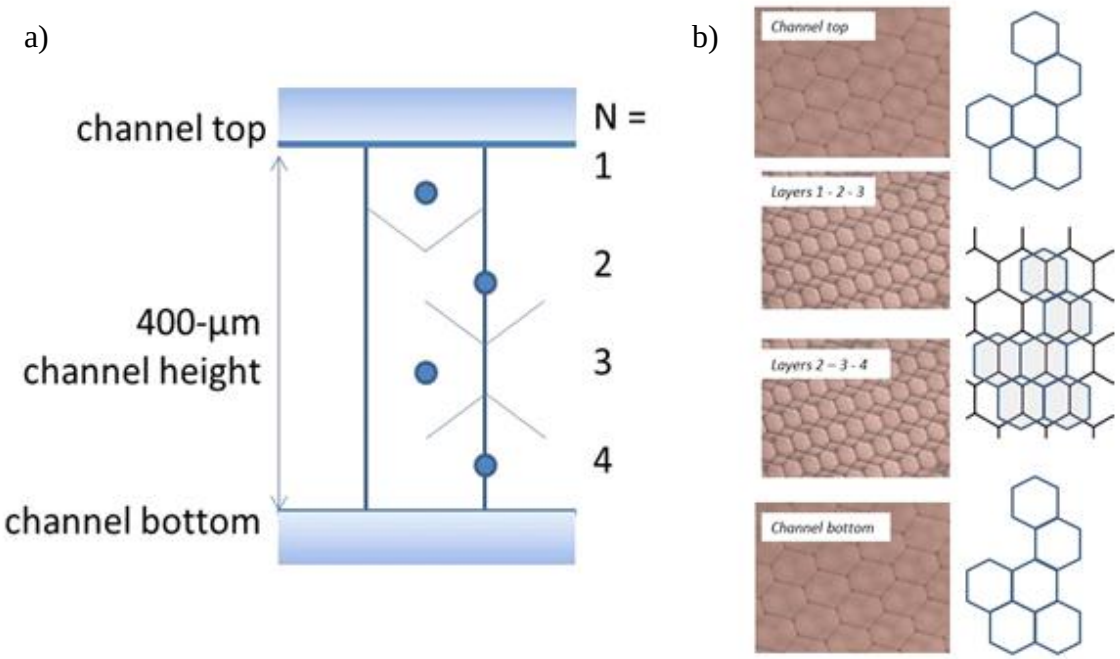

Figure 6. Interpretation of optical microscope images of the emulsion droplet tessellation.
a) Side-view schematic of 100-μm diameter emulsion droplets forming a stack within a 400-μm microfluidic channel height.
b) Focusing through the channel reveals a simple hexagonal pattern at the top and bottom of the channel and the alternating tessellation at the three droplet interfaces, thus confirming the four-layer model.

Since N_L = 4 and h = 393.3 ±2.1 μm are independently determined, only a measurement of the mean hexagonal area, $\bar{A}_{HEX}$, is needed in order to estimate the mean hexagonal volume, $\bar{V}_{HEX}$. The area is obtained from a (Z axis) stack of 10X optical images recorded a dozen or more locations along the microfluidic channel at which large-scale lattice domains are found. The area of a regular hexagon of edge length a can be calculated as $A_{HEX} = \frac{3}{2}\sqrt{3} \cdot a^2$. However, the lattice cell may be slightly distorted and the edge length is then not a reliable parameter. So instead of basing an area determination on measurement of individual hexagonal cells, the average area within a given domain is obtained by defining a boundary around a set of N hexagons, computing the total area using ImageJ [9], and then dividing the total area by N. We refer to this average as $\bar{A}_{HEX}$. Averaging the first and fourth layers was found to yield results essentially identical to averaging data for all four layers; for simplicity we generally report first and fourth layer averaging only. Each area-averaged location contains a contiguous set of ≥20 unit cell positions which was delineated and processed in ImageJ. At each location, $\bar{A}_{HEX}$ was calculated for each group of unit cells. Since a typical volume estimate includes at least 3 days × 4 channels × 6 locations × 4 layers × 20 droplets, the total number of droplets averaged by this method is ≥ 5,760 droplets.

Determination of the volume fraction

So far, we have described the calculation of $\bar{V}_{HEX} = h \cdot \bar{A}_{HEX}/N_L$. In order to accurately determine the quantity of interest, the mean spherical droplet volume in solution or $\bar{V}_{SPH} = \varphi_D \cdot \bar{V}_{HEX}$, we must estimate the volume fraction of the aqueous phase within the hexagonal unit cell, φ_D.

The volume fraction φ_D can be defined in terms of V_{PB}, the volume of continuous (oil) phase remaining trapped at Plateau border channels, the vertices and edges of the hexagonal unit cell. Since the volume of the hexagonal unit cell is $\bar{V}_{HEX}$, $\varphi_D = (1 - V_{PB}/\bar{V}_{HEX})$. The presence of even a small amount of continuous (oil) phase can be inferred from the inherent stability of the hexagonal lattice structure, as discussed below. Optical images shown in Figure 5**,** in which oil in Plateau borders appears with a dark contrast and water is transparent, indicate that the triangular intersections at which four droplets meet decrease in size and contrast as $\varphi_D \rightarrow 1$. Much theoretical and experimental work has gone into establishing a quantitative understanding of how geometric transformations are related to the equilibration of droplet forces in compression [6,7,8].

Our estimation of φ_D relies on the work of Princen [6,7]. A particularly interesting point is that Princen derived results for a 2D hexagonal system as well as for a 3D bulk model. Given that $N_L = 4$, as indicated in Figure 6a, the 2D model very closely conforms to the geometry of our system. More significantly, since the theoretical 2D and 3D volume fractions converge as $\varphi_D \rightarrow 1$, the actual volume fraction is expected to lie somewhere in between. Princen's 2D model consists of a pair of volume-fraction dependent parameters, R/a and r/a where R and r represent a dimensionless droplet radius and its curvature during compression into a regular hexagon of edge length a. These quantities are defined in Figure 7**.**

We now use the factor r/a to obtain estimates for φ_D. The curvature r/a can be scaled to the (isosceles) triangle length at the droplet intersection as shown in Figure 7b. Princen's 2D model, however, yields a dimension for an *uncollapsed* draining channel, where collapse refers to point at which the draining forces have squeezed out all but a negligible amount of oil phase from between adjacent droplets. This calculation is represented by the trigonal prism shown in Figure 7c and therefore overestimates the volume V_{PB}.

However, we require the volume after collapse, i.e., at the quasi-equilibrium condition at which the forces due to external pressure and surface energy are balanced. Plateau border channels in this case appear as tetrahedra located at the vertices of the truncated octahedral Kelvin cell, Figure 7d. This quasi-equilibrium region is illustrated in Figure 8.

For the series of optical micrographs of emulsion draining shown in Figure 5**,** estimates for volume fraction as obtained from r/a are given in Figure 9. Draining of the oil phase is evidently associated with structural transitions of the droplets from spherical to polygonal.

Calculating the oil volume at vertices of Kelvin cells and end caps, and given the number of vertices/per unit cell, the 2D and 3D Princen models indicate that $96.5\ \% < \varphi_D < 99\ \%$. Our estimate for volume fraction of the aqueous phase φ_D is $98 \pm 1\ \%$.

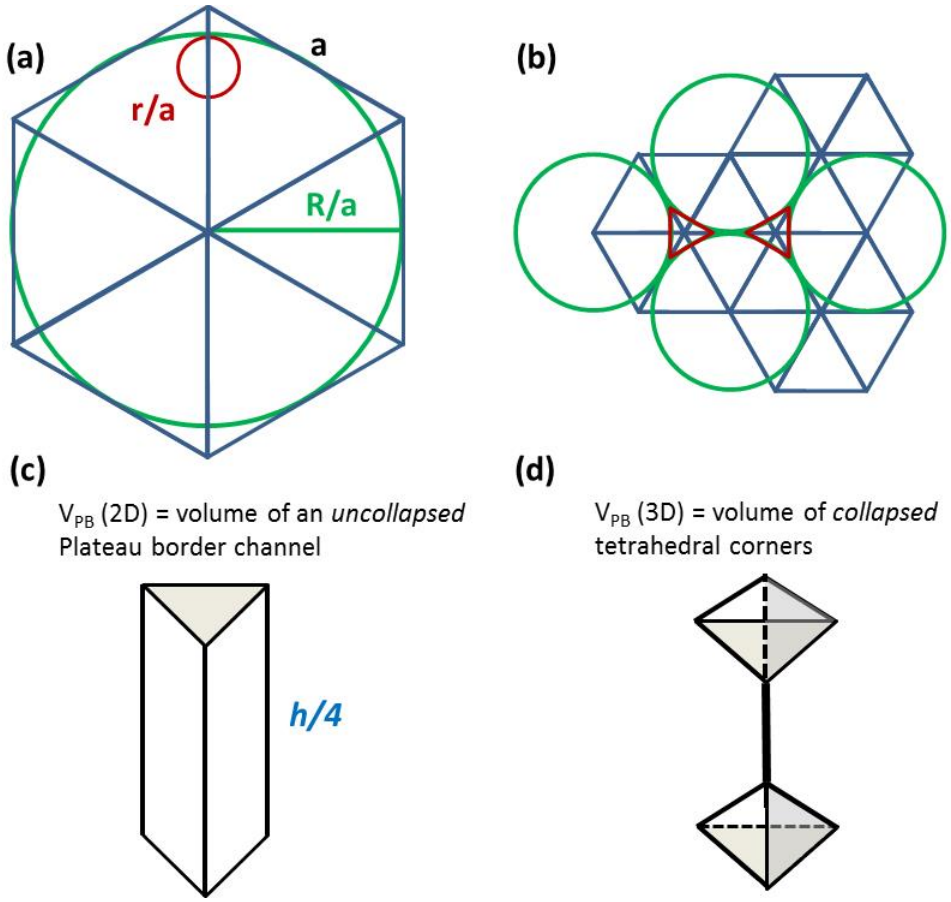

Figure 7. Determination of the volume fraction using Princen's model

a) Definition of the parameters in Princen's 2D model [6].
b) Triangular droplet intersections for a 2D projection.
c) In 2D, the volume of a Plateau border channel $V_{PB} = \frac{h}{4} \cdot a^2$ overestimates the oil phase.
d) In 3D, a collapsed border channel can be represented by $V_{PB} = a^3/6 \cdot \sqrt{2}$, the tetrahedral volume.

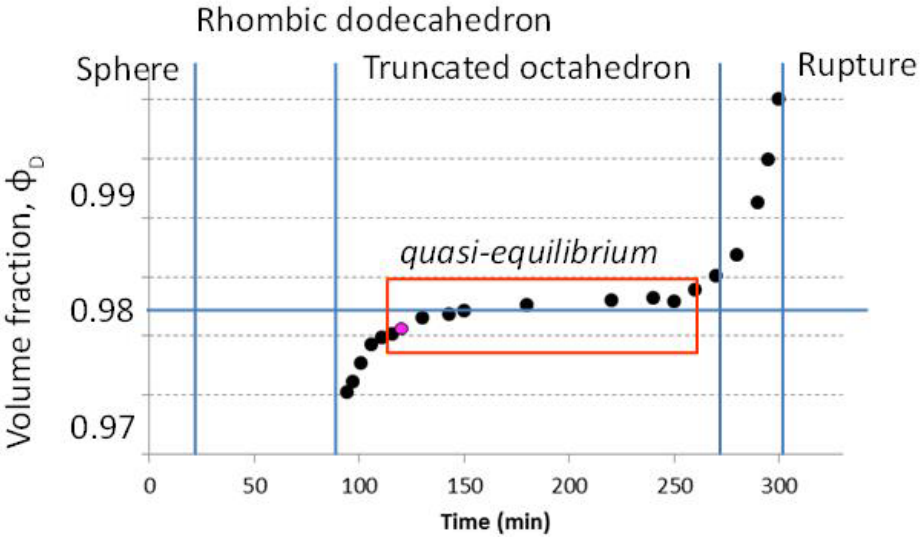

Figure 8. Measurement of the hexagonal unit cell under quasi-equilibrium conditions.

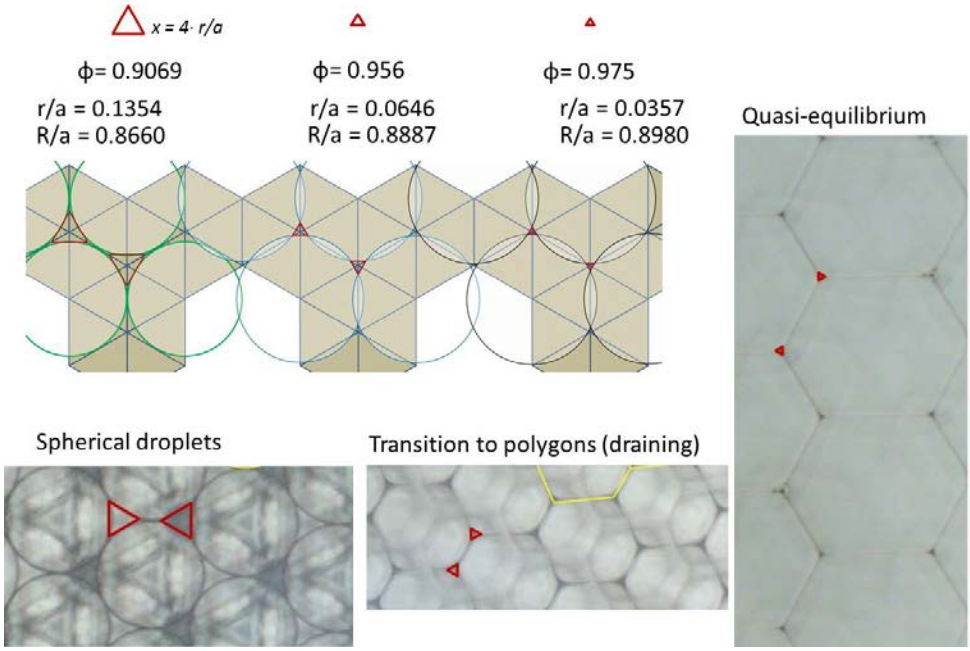

Figure 9. Relationship between volume fraction and curvature parameter, *r*/*a*

Assumption of constant droplet volume

Droplet compression at constant volume involves a transition from spherical shape to space-filling polygons. The process by which this occurs has long been investigated as a function of increasing volume fraction, φ, in terms of geometrical and force equilibration requirements [6,7,8]. The measurement process proposed here relies on a mean droplet volume determination from the polygonal lattice once the maximum amount of continuous (oil) phase drains from the emulsion at ambient conditions; this is referred to as collapse of the Plateau border, which occurs for φ > 96 %. It takes about 2 hours to reach this stage under ambient conditions and the lattice remains stable for a period of several hours. If this shape transition at constant volume is reversible, then adding solvent (oil) to the system during this period should return the droplets to the initial spherical shape and diameter.

The reversibility of the spherical-to-polyhedral shape transition illustrated in Figure 5 was verified as follows. First, the diameter of spherical droplets was measured within the first several minutes of channel filling, i.e., prior to the shape transition into a hexagonal unit cell. After hexagonal domains had been allowed time to form due to sufficient draining, approximately 2 hours, an additional volume of pure oil phase was introduced into the microfluidic channel, restoring droplets to their spherical form. Then measurements of the spherical diameter were obtained for these re-solvated droplets. No detectible difference in the spherical diameter between initial and re-solvated droplets was found.

The unit cell as a quasi-equilibrium structure

The unit cell, the principle measurement model of droplet volume, is actually a metastable structure since the emulsion collapses eventually. It is essential therefore to verify that the measured structures are in a physically meaningful steady-state (or quasi-equilibrium configuration) between draining and coalescence. That this condition is met for the measurement process is illustrated in Figure 8. The theoretical volume fraction is estimated from the change in mean droplet volume as a function

of time according to Princen's model [6,7]. Recording of data commences at about 90 minutes when it becomes possible to measure the tessellating layers and end caps. At that time draining has already pushed the system toward $\varphi_D = 0.965$. Our measurements begin after 2 hours, i.e., along the flat region of the curve and end before the final compression and loss of remaining oil phase that sets in, after about 5 hours. During this time the Plateau borders have collapsed and the external pressure is insufficient to force additional oil out of the interstitial pockets, at least for an additional few hours.

Measurement results and their standard deviations for the mean spherical volume of emulsion droplets are given in Table 7: Summary of mean spherical droplet volume as $\overline{V}_{SPH} = \varphi D \cdot \overline{V}_{HEX}$ measurements. The results are broken down according to protocol: mastermix (with dUTP vs. no dUTP) and DNA source (human genomic vs. CMV). There are no significant differences in droplet volume between the human and viral DNA. However, the volume difference between mastermixes is significant.

Table 7: Summary of mean spherical droplet volume as $\bar{V}_{SPH} = \varphi D \cdot \bar{V}_{HEX}$ measurements

Mastermix;DNA	Samples	Number plates	Number Channels	Number Locations	Number Droplets	Volume Mean ±SD, nL
With dUTP; Human genomic	645-1-12/19/2014 645-1-03/17/2015 645-1-03/20/2015	7	8	59	4720	0.8017 ±0.0037
With dUTP; CMV	645-3-02/24/2015 645-3-02/27/2015 645-3-03/03/2015	8	12	72	5760	0.8064 ±0.0059
With dUTP		15	20	141	10480	0.8041 ±0.0048
No dUTP; Human genomic	645-2-02/04/2015 645-2-02/10/2015 645-2-02/12/2015	7	12	72	5760	0.7681 ±0.0074
No dUTP; CMV	645-4-03/11/2015 645-4-03/12/2015	5	7	14	1120	0.7657 ±0.0032
No dUTP		12	19	86	6880	0.7669 ±0.0053

UNCERTAINTY ANALYSIS

Dilute method

Measurement uncertainty in the case of the dilute method was assumed to depend principally on pixel calibration and droplet boundary determination, i.e., edge location of the spherical droplet. The pixel calibration uncertainty at 10X is 0.1 %. The contribution from edge location was estimated from optical image cross sections of apparently contacting spheres as shown in Figure 4a. Analysis of the slope of grayscale intensity values indicates that the exact droplet boundary could occur across a region of approximately ±4 pixels for each droplet edge, or ±8 pixels per droplet. At 10X each pixel corresponds to 0.394 μm, so that the region spans 3.15 μm. For an average droplet this is 100×3.15 μm/116.1 μm, or 2.7 %.

An estimate of the relative uncertainty arising from the finite width of the droplet size distribution of 0.38 % was obtained from the lognormal width parameter calculated for data from 866 individual droplet measurements summarized in Figure 4b.

Table 8 summarizes the uncertainty budget for this method.

Table 8: Uncertainty budget for dilute method of determining mean droplet diameter

Component	x	$u(x)$	$\%u(x)$[a]	Distribution
1 Pixel calibration @ 10X	0.3943 μm	0.0004 μm	0.10 %	Uniform
2 Edge location of spherical droplets	116.1 μm	3.15 μm	2.7 %	Uniform
3 Droplet size distribution	116.1 μm	0.44 μm	0.38 %	Uniform

a $\%u(x) \equiv 100 \cdot u(x)/x$

The combined relative standard uncertainty for the dilute method is:

$$\%u_{\text{dilute}} = \sqrt{\frac{1}{3}} \sqrt{\sum_{i=1}^{3} \%u^2(x_i)} = 2.73/1.73 = 1.6\ \%$$

where $u(x_i)$ are normal-distribution standard uncertainties of the components as listed in Table 8 and the factor $\sqrt{1/3}$ converts them to represent normal-distribution estimates. [17] Using a coverage factor of $k = 2$, the expanded relative uncertainty is then

$$\%U_{k=2} = 2 \cdot \%u_{\text{dilute}} = 3.2\ \% .$$

Table 10 compares results of the dilute and concentrated methods.

However, estimates based on spherical droplet diameters are sensitive to the dilution environment. This introduces considerable uncertainty into the measurement since the draining of the oil phase around the droplets affects optical contrast at the droplet periphery as well as leading to non-spherical droplet shapes. These potential sources of variability and bias are not accounted for in the above budget.

Concentrated method

To estimate an expanded uncertainty for the measurement of the mean spherical volume of emulsion droplets for the concentrated method, both Type A and Type B uncertainty components are evaluated. Type A components are associated with an analysis of empirical measurement data according to statistical means and Type B estimates are concerned with the capability of a proposed measurement process to realize an abstract measurand.

Hierarchical ANOVA [18] analysis was performed to discern any significant impact of day-to-day sample preparation, manufacture of the microfluidic plates, and, measurement repeatability and reproducibility. The resulting Type A estimates are characterized as normal distributions in Table 9. The remaining sources of variability and bias are treated as Type B uniform distributions. These uncertainty components are described more fully below and are summarized in Table 9.

Type A: Sample emulsion preparation
The emulsion-forming process may be sensitive to a number of physical and chemical variations arising from volume and the choice of constituents in the proprietary mixes used in the preparation of the emulsion. The ANOVA component for this source of error appears as entry 1 in Table 9.

Type A: Manufacturing
Qualification of the specific lot of plates is treated below as a Type B uncertainty, so we are primarily concerned here with identifying potential variations which might lie outside the expected tolerances. The ANOVA component for this source of error appears as entry 2 in Table 9. Similarly, the traceable determination of the height of the microfluidic channel is also calibrated and determined as a separate Type B uncertainty below and is established for the specific lot of plates used in these measurements.

Type A: Measurement
Measurement and analysis of hexagonal unit cells is largely an operator-intensive effort to identify locations within a channel with a high degree of lattice perfection. The hexagonal area of individual unite cells may be subject to layer-by-layer variations and geometric distortion of polygons. These are expected to average out over a large number of unit cells and droplets and use of the ANOVA technique is an effort to validate this assumption. The ANOVA component for this source of error appears as entry 3 in Table 9.

Type B: Sample size distribution
The sample size distribution produced by the emulsion system is distinct from the day-to-day variability of sample preparation which may result from pipetting and so forth. It is considered a possible Type B uncertainty. As reported for the dilute method, the standard deviation of the droplet size distribution is 0.44 μm, based on the results shown in Figure 4. It appears as entry 4 in Table 9.

Type B: Pixel calibration
This estimate is also carried over from the dilute method and appears as entry 5 in Table 9.

Type B: Estimation of $\bar{V}_{\mathrm{HEX}}$
The measurand $\bar{V}_{\mathrm{SPH}} = \varphi_{\mathrm{D}} \cdot \bar{V}_{\mathrm{HEX}}$, is an idealized model of the actual measurement data. The uncertainty evaluation is presented in two parts. We first evaluate the uncertainty components arising from the calculation of $\bar{V}_{\mathrm{HEX}} = h \cdot \bar{A}_{\mathrm{HEX}} / N_{\mathrm{L.}}$

The major component of uncertainty due to measurement is the traceable determination of the channel height, *h*, which was found to be about 0.13 %. It appears as entry 6 in Table 9. This uncertainty could be reduced if local measurement values were used instead of a single global value. However, its contribution is small enough for the intended use. N_L = 4 is considered an errorless constant as it is always observed for well-formed droplet domains. It appears as entry 7 in Table 9.

For the estimation of an average hexagonal area, we do not use lattice parameters. Compressive forces acting on the droplets are not purely isotropic, so that a 3D polygonal lattice is not necessarily definable by a single hexagonal edge length *a* across the domain. Absolute lattice constants can only be guaranteed if the droplets are incompressible. For this reason, we do not calculate the area of a hexagonal unit cell based on based on $A_{HEX} = \frac{3}{2}\sqrt{3} \cdot a^2$. Rather, optical images indicate that hexagonal domains are distorted by lateral or vertical skewing or subject to shearing along the channel boundaries. Therefore, averaging a large number of contiguous unit cells by defining a boundary around a set of *N* hexagons and computing the total area using ImageJ provides a reliable estimate of the mean unit-cell area within a given domain. Repeatability of image analysis to determine $\bar{A}_{HEX}$ in this manner was found to be ± 0.017 %. This contribution appears as entry 8 in Table 9.

Type B: Manufacturing
Components of uncertainty arising from channel roughness, form errors, and dimensional conformance of the microfluidic channel are evaluated from WYKO and optical measurements of a large number of ibidi channel plates from the same lot number.

Channel roughness was determined from the root-mean-square (RMS) surface roughness of the top exposed surface of intact membranes and mechanically grooved channels using WYKO analysis software. This error was calculated to be about 0.2 % of the channel height measurement, close to the resolution limit of the instrument, and appears as entry 9 in Table 9.

Since the channel membrane has a thickness of only about 200 μm, it is possible that channels do not possess a uniform rectangular cross section. This may be due to deformation of the membrane during manufacturing or arise from compressive forces as the concentrated fluid dries within the channel. Flatness across empty and filled channels was estimated to be less than 0.2 % based on WYKO data as shown on the right hand side of Figure 2, close to the resolution limit of the instrument. It appears as entry 10 in Table 9.

Uniformity of the channel cross section was also evaluated in terms of a difference between the left and right channel height as shown on the left hand side of Figure 2. Some differences are apparent from the total height measured across the ibidi plate. The variations are an aspect of manufacturing and, as noted earlier, by avoiding the use of channels 1 and 6, deviations from a rectangular geometry are small. This component is estimated by comparing difference between left/right channel data presented in Tables 3 to 5 and appears as entry 11 in Table 9.

Type B: Volume fraction
The uncertainty related to the volume fraction, $\varphi_{D,}$ represents the largest uncertainty contribution to $\bar{V}_{SPH}$ since it is must be estimated by interpolating between Princen's 2D and 3D theoretical models. Nevertheless, the calculated expanded uncertainty, *U*, lies within the range required by the intended use. It appears as entry 12 in Table 9.

Table 9: Uncertainty budget for concentrated method of determining mean droplet diameter

Component	x	$u(x)$	$\%u(x)$[a]	Distribution
1 Sample preparation			0.064 %	Normal
2 Manufacturing			0.022 %	Normal
3 Measurement			0.044 %	Normal
4 Droplet size distribution	116.1 µm	0.44 µm	0.38 %	Uniform
5 Pixel calibration	0.3943 µm	0.0004 µm	0.10 %	Uniform
6 Channel height, h	393.3 µm	2.1 µm	0.13 %	Uniform
7 Channel number, N_L	4	0	0.0 %	Uniform
8 Estimation of $\bar{A}_{HEX}$			0.017 %	Uniform
9 Channel roughness			0.02 %	Uniform
10 Form errors			0.2 %	Uniform
11 Left/Right channel conformance			0.2 %	Uniform
12 Volume fraction, φ_D	0.98	0.01	1 %	Normal

a $\%u(x) \equiv 100 \cdot u(x)/x$

Combined Relative Standard Uncertainty

The uncertainty estimate for the mean droplet volume can be performed as follows. Note that Type A and Type B components are expressed in linear dimensions. This is consistent with the view that traceability is fundamentally established through a calibrated measurement of the microfluidic channel height. The combined relative standard uncertainty of the Type A components for the droplet diameter is:

$$\%u_A(d) = \sqrt{\sum_{i=1}^{3} \%u^2(x_i)} = 0.081\ \%$$

where $u(x_i)$ are normal-distribution standard uncertainties of the components 1 to 3 listed in Table 9. The combined relative standard uncertainty of the Type B components is:

$$\%u_B(d) = \sqrt{\frac{1}{3}} \sqrt{\sum_{i=4}^{11} u^2(x_i)} = \frac{0.50}{1.73} = 0.29\ \%$$

where $u(x_i)$ are uniform-distribution relative standard uncertainties of the components 1 to 3 listed in Table 9 and the factor $\sqrt{1/3}$ converts them to represent normal-distribution estimates. The complete combined relative standard uncertainty of the droplet diameter measurements is then:

$$\%u(d) = \sqrt{u_A^2(d) + u_B^2(d)} = \sqrt{0.081^2 + 0.29^2} = 0.30\ \%.$$

Assuming a coverage factor of $k = 2$, an expanded relative uncertainty for the droplet diameter estimated in this manner is

$$\%U_{k=2}(d) = 2 \cdot \%u(d) = 0.60\ \%$$

which is substantially less than the 3.2 % relative expanded uncertainty calculated for the dilute method.

What we desire is the combined uncertainty of the equivalent spherical droplet volume,

$$\bar{V}_{\mathrm{SPH}} = \varphi_D \cdot \bar{V}_{\mathrm{HEX}},$$

where

$$\bar{V}_{\mathrm{HEX}} = \left(\frac{4}{3}\right)\pi\left(\frac{d}{2}\right)^3 = \left(\frac{\pi}{6}\right)d^3.$$

A linearized model* for the combined relative uncertainty of $\bar{V}_{\mathrm{HEX}}$ is

$$\frac{u(\bar{V}_{\mathrm{HEX}})}{\bar{V}_{\mathrm{HEX}}} = 3 \cdot \frac{u(d)}{d}.$$

Given the 0.30 % value for $\%u(d)$ calculated above and recognizing that

$$\%u(\bar{V}_{\mathrm{HEX}}) \equiv 100 \cdot \frac{u(\bar{V}_{\mathrm{HEX}})}{\bar{V}_{\mathrm{HEX}}} \text{ and } \%u(d) \equiv 100 \cdot \frac{u(d)}{d},$$

the percent relative standard uncertainty of the volume is

$$\%u(\bar{V}_{\mathrm{HEX}}) = 3 \cdot \%u(d) \;=\; 3 \cdot 0.30\,\% = 0.90\,\%.$$

From Table 9, the volume fraction is $\varphi_D = 0.98 \pm 0.01$ with a combined relative standard uncertainty of $\%u(\varphi_D)$ = 1.0 %, so the linearized model yields

$$\%u(\bar{V}_{\mathrm{SPH}}) = \sqrt{\%u^2(\varphi_D) + \%u^2(\bar{V}_{\mathrm{HEX}})} \;= \sqrt{1.0^2 + 0.90^2} = 1.4\,\%$$

for the combined relative standard uncertainty of the spherical volume. Assuming a coverage factor of k = 2, an expanded relative uncertainty for the droplet volume measurement is then

$$\%U_{k=2}(\bar{V}_{\mathrm{SPH}}) = 2 \cdot \%u(\bar{V}_{\mathrm{SPH}}) = 2 \cdot 1.4\,\% = 2.8\,\%.$$

While reflecting the uncertainty component estimates listed in Table 9, this expanded uncertainty should be appropriate for droplets formed from both the “with dUTP” and “no UTP” mastermixes.

* First-order Taylor series expansion: $y = f(x)$; $u(y) = \sqrt{\sum\left(\frac{\partial f}{\partial x}\right)^2 \cdot u^2(x)}$

VALIDATION

Comparison of Results from the Dilute and Concentrated Methods

Table 10 compares estimates of droplet diameter from the dilute and concentrated methods. The diameter is obtained directly in the dilute method, whereas the volume is obtained first in the concentrated method.

Table 10: Comparison of mean emulsion droplet diameter
All values in μm

		Dilute Method		Concentrated Method	
Mastermix;DNA	Sample	Value	Mean ±SD	Value	Mean ±SD
With dUTP; human genomic	645-1-12/19/2014 645-1-03/17/2015 645-1-03/20/2015	116.1 115.5 116.3	116.0 ±0.4	116.0 115.9 116.1	116.0 ±0.1
With dUTP; CMV	645-3-02/24/2015 645-3-02/27/2015 645-3-03/03/2015	115.5 115.9 116.0	115.8 ±0.3	115.6 116.6 116.6	116.3 ±0.6
With dUTP			115.9 ±0.3		116.1 ±0.4
No dUTP; human genomic	645-2-02/04/2015 645-2-02/10/2015 645-2-02/12/2015	113.7 114.3 114.5	114.2 ±0.4	113.8 114.8 114.6	114.4 ±0.5
No dUTP; CMV	645-4-03/11/2015 645-4-03/12/2015	na 114.1	114.1	114.2 114.4	114.3 ±0.1
No dUTP			114.2 ±0.3		114.4 ±0.4

Droplet diameter estimates obtained by dilute and concentrated methods agree reasonably well, indicating that the possibly simpler dilute method can be used to establish, or assess, volume and DNA concentration. The significant difference between the “with dUTP” and “no dUTP” mastermixes extends to the dilute method.

Comparison with Literature Results

The present results are validated against previously published work in Table 11.

Table 11: Evolution of mean droplet diameter and volume estimates

Source	Date	Diameter, μm	Volume, nL
Nominal		124.0	1.000
Bio-Rad [1]	2009	120.2	0.910
NMIA [4]	2012	118.4	0.868
IRMM [3]	2015	116.8	0.834
NIST, Dilute method, with dUTP NIST, Dilute method, no dUTP	2015 2015	115.9 114.2	0.815 0.780
NIST, Concentrated method, with dUTP NIST, Concentrated method, no dUTP	2015 2015	116.1 114.4	0.804 0.767

There is a trend toward lower volume estimates, and therefore higher DNA concentration values, as refinements to the emulsifying system and its software occurred. In addition, larger sets of droplet measurement data obtained under more controlled conditions have appeared. However, a persistent discrepancy between DNA concentration estimates based on ddPCR and other methods remain. This has been discussed in the literature recently [see the discussion of Figure 4 of Reference 3]. We expect that volume estimates reported in this work will reduce or eliminate this discrepancy.

REFERENCES

[1] Bio-Rad Laboratories Inc., Pleasanton, CA, USA. (http://www.bio-rad.com/en-us/applications-technologies/introduction-digital-pcr)

[2] Ibidi LLC, Verona, WI, USA. (http://ibidi.com/xtproducts/en/ibidi-Labware/Channel-Slides/m-Slide-VI-Flat)

[3] P. Corbisier et al., DNA copy number concentration measured by digital and digital quantitative PCR using certified reference materials, Anal. Bioanal. Chem. 407 1831 (2015).

[4] L. B. Pinheiro et al., Evaluation of a droplet digital polymerase chain reaction format for DNA copy number quantification, Anal. Chem. 84 1003 (2012).

[5] S. Bhat et al., Single molecule detection in nanofluidic digital array enables accurate measurement of DNA copy number, Anal. Bioanal. Chem. 394 457 (2009).

[6] H. M. Princen, Highly concentrated foams, I. Cylindrical systems, J. Coll. Interface Sci. 71 55 (1979).

[7] H. M. Princen, M. P. Aronson, and J. C. Moser, Highly concentrated emulsions, II. Real systems, J. Coll. Interface Sci. 75 246 (1980).

[8] A. Bhakta and E. Ruckenstein, Decay of standing foams: drainage, coalescence and collapse, Adv. Coll. Interface Sci. 70 1 (1997).

[9] ImageJ v1.47, available from the National Institutes of Health. (http://rsbweb.nih.gov/ij/)

[10] SRM 1690 – Nominal One-µm Polystyrene Spheres.
(https://www-s.nist.gov/srmors/certificates/archive/1690.%20Dec%2022,%201982.pdf)

[11] SRM 1692 - Polystyrene Spheres (3 µm Diameter Particle Size).
(https://www-s.nist.gov/srmors/view_cert.cfm?srm=1692)

[12] Paraphrased from: WYKO Surface Profilers Technical Reference Manual, 1998.

[13] SRM 2390 – DNA Profiling Standard.
(https://www-s.nist.gov/srmors/certificates/archive/2390.%20Aug%2010,%201992.pdf)

[14] SRM 2366a - Cytomegalovirus DNA (TowneΔ147 BAC) for DNA Measurements.
(https://www-s.nist.gov/srmors/view_detail.cfm?srm=2366a)

[15] ddPCR Supermix for Probes #186-3010.
(http://www.bio-rad.com/en-us/sku/1863010-ddpcr-supermix-for-probes)

[16] ddPCR Supermix for Probes (no dUTP) #186-3024.
(http://www.bio-rad.com/en-us/product/ddpcr-supermix-for-probes-no-dutp)

[17] JCGM 100:2008 (2008) Guide to the expression of uncertainty in measurement (GUM). Sèvres, France. (http://www.bipm.org/utils/common/documents/jcgm/JCGM_100_2008_E.pdf)

[18] G. E. P. Box and G. C. Tiao, Bayesian Inference in Statistical Analysis, John Wiley and Sons, Inc., New York (1992), Chapter 5.